New Measurement of the Electron Magnetic Moment Using a One-Electron Quantum Cyclotron

B. Odom,* D. Hanneke, B. D'Urso,† and G. Gabrielse‡

Department of Physics, Harvard University, Cambridge, Massachusetts 02138, USA

(Received 17 May 2006; published 17 July 2006)

A new measurement resolves cyclotron and spin levels for a single-electron quantum cyclotron to obtain an electron magnetic moment, given by $g/2 = 1.001\,159\,652\,180\,85\,(76)$ [0.76 ppt]. The uncertainty is nearly 6 times lower than in the past, and g is shifted downward by 1.7 standard deviations. The new g, with a quantum electrodynamics (QED) calculation, determines the fine structure constant with a 0.7 ppb uncertainty—10 times smaller than for atom-recoil determinations. Remarkably, this 100 mK measurement probes for internal electron structure at 130 GeV.

DOI: 10.1103/PhysRevLett.97.030801 PACS numbers: 06.20.Jr, 12.20.Fv, 13.40.Em, 14.60.Cd

Measurements of the electron magnetic moment ($\boldsymbol{\mu}$) probe the electron's interaction with the fluctuating vacuum of QED, and also probe for possible electron substructure. As an eigenstate of spin $\mathbf{S}$, the electron (charge $-e$ and mass m) has $\boldsymbol{\mu} \propto \mathbf{S}$,

$$\boldsymbol{\mu} = -g\frac{e\hbar}{2\mathrm{m}}\frac{\mathbf{S}}{\hbar}. \quad (1)$$

The constant g is a dimensionless measure of the moment, with the dimensions and approximate size given by the Bohr magneton, $e\hbar/(2m)$. If the electron was a mechanical system with an orbital angular momentum, then g would depend upon the relative distributions of the rotating charge and mass, with $g = 1$ for identical distributions. [Cyclotron motion of a charge in a magnetic field B, at frequency $\nu_c = eB/(2\pi m)$, is one example.] A Dirac point particle has $g = 2$. QED predicts that vacuum fluctuations and polarization slightly increase this value. Electron substructure [1] would make g deviate from the Dirac-QED prediction (as quark-gluon substructure does for a proton).

Measurements of the electron g have a long history [2,3], with a celebrated measurement [4] providing the accepted value [5] since 1987. The new g has a 6 times smaller standard deviation and is shifted by 1.7 standard deviations [Fig. 1(a)]. A one-electron quantum cyclotron [6], cavity-inhibited spontaneous emission [7], a self-excited oscillator (SEO) [8], and a cylindrical Penning trap [9] contribute to the extremely small uncertainty. For the first time, spectroscopy is done with the lowest cyclotron and spin levels of a single electron fully resolved via quantum nondemolition (QND) measurements [6], and a cavity shift of g is directly observed.

What can be learned from the more accurate electron g? The first result beyond g itself is the fine structure constant, $\alpha = e^2/(4\pi\epsilon_0\hbar c)$, determined from g and QED with 10 times smaller uncertainty compared to any other method [10–12]. This fundamental measure of the strength of the electromagnetic interaction is a crucial ingredient in our system of fundamental constants [5]. Second, the most demanding test of QED continues to be a comparison of measured and calculated g, and the way is now prepared for a 10 times more stringent test. Third, even though muon g values [13] have nearly 1000 times larger uncertainties compared to the electron g, heavy particles (possibly unknown in the standard model) make a contribution that is relatively much larger for the muon. However, the contribution is small compared to the calculated QED contribution which depends on α and must be subtracted out. The electron g provides α and a confidence-building test of the required QED.

The electron g determines the spin frequency $\nu_s = \frac{g}{2}\nu_c$ for a free electron in a magnetic field $B\hat{\mathbf{z}}$. To weakly confine the electron, an electric quadrupole potential, $V \sim 2z^2 - \boldsymbol{\rho}^2$, is added, with $\boldsymbol{\rho} = x\hat{\mathbf{x}} + y\hat{\mathbf{y}}$. Optimal biasing of the electrodes [Fig. 2(a)] of an orthogonalized cylindrical Penning trap [9] minimizes an undesired z^4 term. The electron-trap system has four eigenfrequencies. The spin and trap-modified cyclotron frequencies are approximately equal at $\nu_s \approx \bar{\nu}_c \approx 149$ GHz. A harmonic axial oscillation along $\mathbf{B}$ is at $\bar{\nu}_z \approx 200$ MHz, and an orthogonal circular magnetron oscillation is at $\bar{\nu}_m \approx 134$ kHz. The latter three frequencies are shifted by the unavoidable leading imperfections of a real Penning trap—harmonic distortions of the quadrupole potential, and a misalignment of the electrode axis and $\mathbf{B}$ [14]. Silver trap electrodes were used after the nuclear paramagnetism of copper electrodes caused unacceptable temperature-dependent fluctuations in $\mathbf{B}$ near 100 mK.

The spin motion is undamped, being essentially uncoupled from its environment [15]. The cyclotron motion

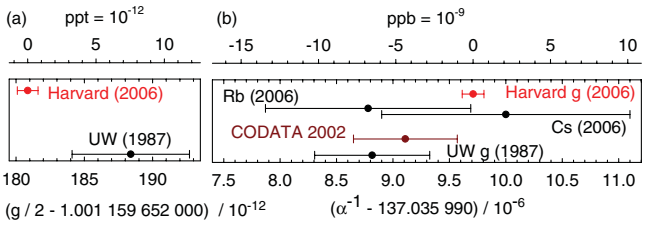

FIG. 1 (color). Measurements of the electron g (a). Determinations of α [11,12], and the current CODATA value [5] (b). Measured g are converted to α with current QED theory.

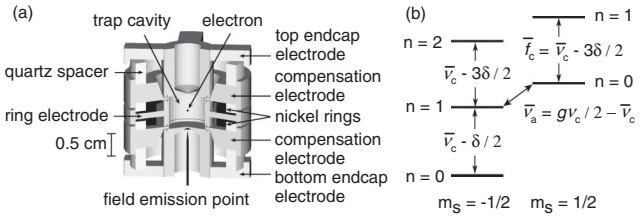

FIG. 2. Cylindrical Penning trap cavity used to confine a single electron and inhibit spontaneous emission (a), and the cyclotron and spin levels of an electron confined within it (b).

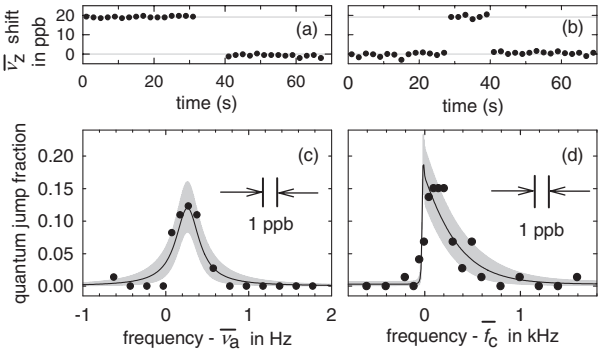

FIG. 3. Sample $\bar{\nu}_z$ shifts for a spin flip (a) and for a one-quantum cyclotron excitation (b). Quantum jump spectroscopy line shapes for anomaly (c) and cyclotron (d) transitions, with a maximum likelihood fit to the calculated line shapes (solid). The bands indicate 68% confidence limits for distributions of measurements about the fit values.

would damp in ~0.1 s via synchrotron radiation in free space. This spontaneous emission is greatly inhibited in the trap cavity (to 6.7 or 1.4 s here) when $\mathbf{B}$ is tuned so $\bar{\nu}_c$ is far from resonance with cavity radiation modes [7,15]. Blackbody photons that would excite the cyclotron ground state are eliminated by cooling the trap and vacuum enclosure below 100 mK with a dilution refrigerator [6]. (Thermal radiation through the microwave inlet makes <1 excitation/h.) The axial motion, damped by a resonant circuit, cools below 0.3 K (from 5 K) when the axial detection amplifier is off for crucial periods. The magnetron motion radius is minimized with axial sideband cooling [15].

For the first time, g is deduced from observed transitions between only the lowest of the spin ($m_s = \pm 1/2$) and cyclotron ($n = 0, 1, 2, \ldots$) energy levels [Fig. 2(b)],

$$E(n, m_s) = \frac{g}{2} h\nu_c m_s + \left(n + \frac{1}{2}\right) h\bar{\nu}_c - \frac{1}{2} h\delta\left(n + \frac{1}{2} + m_s\right)^2. \tag{2}$$

The needed $\nu_c = eB/(2\pi m)$ (for a free electron in a magnetic field) is related to the observable eigenfrequencies by the Brown-Gabrielse invariance theorem [14],

$$(\nu_c)^2 = (\bar{\nu}_c)^2 + (\bar{\nu}_z)^2 + (\bar{\nu}_m)^2, \tag{3}$$

which applies despite the mentioned imperfection shifts of the three eigenfrequencies. The third term in Eq. (2), the leading relativistic correction [15] with $\delta/\nu_c \equiv h\nu_c/(mc^2) \approx 10^{-9}$, would add uncertainty to the measurement if cyclotron energy levels were not resolved.

The anomaly and spin-up cyclotron frequencies [$\bar{\nu}_a \approx$ 173 MHz and $\bar{f}_c$ in Fig. 2(b)] are measured, since

$$\frac{g}{2} = \frac{\bar{\nu}_c + \bar{\nu}_a}{\nu_c} \simeq 1 + \frac{\bar{\nu}_a - \bar{\nu}_z^2/(2\bar{f}_c)}{\bar{f}_c + 3\delta/2 + \bar{\nu}_z^2/(2\bar{f}_c)}. \tag{4}$$

We use the approximation to the right which requires no measurement of $\bar{\nu}_m$. It incorporates an expansion of the invariance theorem [14], using $\bar{\nu}_c \gg \bar{\nu}_z \gg \bar{\nu}_m \gg \delta$. Corrections go as the product of $(\bar{\nu}_z/\bar{\nu}_c)^4 \sim 10^{-12}$ and a misalignment or harmonic distortion factor $\sim 10^{-4}$ [14].

A change in cyclotron or spin state is revealed by $\bar{\nu}_z$ shifts [Fig. 3(a) and 3(b)] of a one-electron SEO [8]. The electron's axial oscillation induces a signal in a resonant circuit that is amplified and fed back to drive the oscillation. QND couplings of spin and cyclotron energies to $\bar{\nu}_z$ [6] arise because saturated nickel rings [Fig. 2(a)] produce a small magnetic bottle, $\Delta\mathbf{B} = \beta_2[(z^2 - \rho^2/2)\hat{\mathbf{z}} - z\rho\hat{\boldsymbol{\rho}}]$ with $\beta_2 = 1540\ \mathrm{T/m^2}$.

Anomaly transitions are induced by applying potentials oscillating at $\bar{\nu}_a$ to electrodes, to drive an off-resonance axial motion through the bottle's $z\boldsymbol{\rho}$ gradient. The electron sees the oscillating magnetic field perpendicular to $\mathbf{B}$ as needed to flip its spin, with a gradient that allows a simultaneous cyclotron transition. Cyclotron transitions are induced by microwaves with a transverse electric field that are injected into and filtered by the cavity. The electron samples the same magnetic gradient while $\bar{\nu}_a$ and $\bar{f}_c$ transitions are driven, because both drives are kept on, with one detuned slightly so that only the other causes transitions.

A measurement starts with the SEO turned on to verify that the electron is in the upper of the two stable ground states, $|n = 0, m_s = 1/2\rangle$. Simultaneous $\bar{\nu}_c - \delta/2$ and $\bar{\nu}_a$ drives prepare this state as needed. The magnetron radius is reduced with 1.5 s of strong sideband cooling [15] at $\bar{\nu}_z + \bar{\nu}_m$, and the detection amplifier is turned off. After 1 s, either an $\bar{f}_c$ drive, or a $\bar{\nu}_a$ drive, is on for 2 s. The detection amplifier and the SEO are then switched on to check for a cyclotron excitation, or a spin flip (from an anomaly transition followed by a cyclotron decay). Inhibited spontaneous emission gives the time needed to observe a cyclotron excitation before an excited state decays. We step through each $\bar{\nu}_c$ and $\bar{\nu}_a$ drive frequency in turn, recording the number of quantum jumps per drive attempt. This measurement cycle is repeated during nighttimes, when electrical and magnetic noise are lower. A low drive strength keeps the transition probability below 20% to avoid saturation effects.

Quantum jump spectroscopy (measuring the quantum jumps per attempt to drive them as a function of drive

frequency) gives resonance line shapes for $\bar{\nu}_a$ and $\bar{f}_c$ [Fig. 3(c) and 3(d)]. For weak drives that avoid saturation, the line shape comes from thermal axial motion within the magnetic bottle [16]. The small coherent axial oscillation at $\bar{\nu}_a$ has no noticeable effect. However, otherwise undetectable ppb fluctuations in **B**, on time scales shorter than an hour, would smear the expected line shapes.

At the first of two magnetic fields used, $\bar{\nu}_c \approx 146.8$ GHz. A 1.4 s damping time gives good line shape statistics [e.g., Fig. 3(c) and 3(d)] with 66 measurement cycles per night on average. Three methods to extract $\bar{\nu}_a$ and $\bar{f}_c$ from line shapes give the same g within 0.6 ppt—our "line shape model" uncertainty in Table I. The first is maximum likelihood fitting of the Brownian motion line shape. The second method fits a convolution of this line shape and a Gaussian resolution function, about 1 ppb wide. The third method weights each drive frequency by the number of quantum jumps it produces, and uses the weighted average frequencies in Eq. (4) for $\bar{\nu}_a$ and $\bar{f}_c$. (Understood shifts proportional to axial temperature, common to both frequencies, do not increase the uncertainty.) This weighted average method should account for Brownian axial motion and additional fluctuations of **B**. At our second field, where $\bar{\nu}_c \approx 149.0$ GHz, the 6.7 s damping time allows only 29 measurement cycles per night on average. A long wait is needed to make certain that a spin flip has not occurred. The weighted averages method is used for the lower statistics line shapes.

The $\bar{\nu}_z$ in Eq. (4) pertains while $\bar{f}_c$ and $\bar{\nu}_a$ are driven—not what is measured when the SEO amplifier is on and increasing the axial temperature from 0.3 to 5 K. Limits on axial heating shifts come from the width of a notch in the noise spectrum resonance for the resonant circuit [15] (Table I), measured less well for $\bar{\nu}_c \approx 146.8$ GHz.

Although the g value from Eq. (4) is independent of **B**, field stability is still an important challenge, since $\bar{\nu}_a$ and $\bar{f}_c$ are measured at different times. After the superconducting solenoid settles for several months, field drifts below 10^{-9}/night have been observed. This requires regulating five He and N_2 pressures in the solenoid and experiment cryostats, and the surrounding air temperature to 0.3 K. We correct for drifts up to 10^{-9}/hr using a cyclotron resonance edge measured once in 3 h.

TABLE I. Applied corrections and uncertainties for g in ppt.

Source $\bar{\nu}_c$ =	146.8 GHz	149.0 GHz
$\bar{\nu}_z$ shift	0.2 (0.3)	0.00 (0.02)
Anomaly power	0.0 (0.4)	0.00 (0.14)
Cyclotron power	0.0 (0.3)	0.00 (0.12)
Cavity shift	12.8 (5.1)	0.06 (0.39)
Line shape model	0.0 (0.6)	0.00 (0.60)
Statistics	0.0 (0.2)	0.00 (0.17)
Total	13.0 (5.2)	0.06 (0.76)

The trap cavity modifies the density of states of radiation modes of free space, though not enough to significantly affect QED calculations of g [17]. However, cavity radiation modes do shift $\bar{f}_c$ [18]—still a significant uncertainty, as in the past [4,18]. We use a synchronized-trapped-electrons method [19] to observe quantitatively understandable radiation modes [Fig. 4(a)] of a good cylindrical Penning trap cavity [9]. Our best measurement comes from choosing $\bar{\nu}_c \approx 149.0$ GHz, maximally detuned from modes that couple to a centered electron's cyclotron motion. A measurement at $\bar{\nu}_c \approx 146.8$ GHz, uncomfortably close to TE_{127}, checks how well cavity shifts are understood. Until the cavity spectrum and its frequency calibration is more carefully studied, TE_{127} and TM_{143} are assumed only to lie within the shaded bands. A renormalized calculation (Eq. 8.19 of [15]) gives a range of possible cavity shifts of the measured g [Fig. 4(b)] that is insensitive to mode quality factors for $Q > 500$. Assigned shifts and uncertainties are indicated in Fig. 4(b) and in Table I. The first direct observation of a cavity shift of g, the difference between our two measurements [Fig. 4(c)], lies within the predicted range.

A new value for the electron magnetic moment,

$$g/2 = 1.001\,159\,652\,180\,85\,(76)\ [0.76\ \text{ppt}], \qquad (5)$$

comes from the measurement at $\bar{\nu}_c \approx 149.0$ GHz. (A weighted average with the more uncertain measurement at $\bar{\nu}_c \approx 146.8$ GHz is larger by 0.06 ppt, with a decreased uncertainty of 0.75 ppt.) The standard deviation, about 6 times smaller than from any previous measurement, arises mostly from the line shape model and cavity shifts (Table I). Varying the $\bar{\nu}_a$ and $\bar{f}_c$ drive power causes no detectable shifts of g.

QED provides an asymptotic series relating g and α,

$$\frac{g}{2} = 1 + C_2\left(\frac{\alpha}{\pi}\right) + C_4\left(\frac{\alpha}{\pi}\right)^2 + C_6\left(\frac{\alpha}{\pi}\right)^3 + C_8\left(\frac{\alpha}{\pi}\right)^4 + \ldots + a_{\mu\tau} + a_{\text{hadronic}} + a_{\text{weak}}, \qquad (6)$$

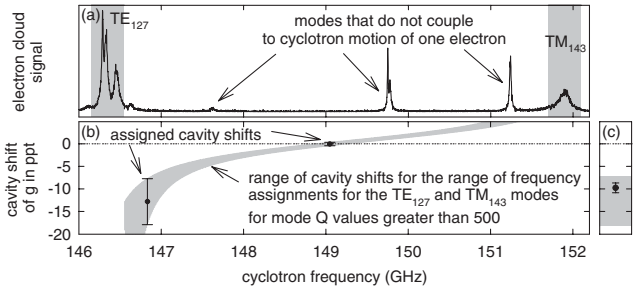

FIG. 4. Modes of the trap cavity observed with synchronized electrons (a). Resulting assigned cavity shifts (points and Table I) (b). First measured cavity shift of g (point) is the shift between measurements at 146.8 and 149.0 GHz (c). Gray bands are the assumed calibration and identification uncertainties for mode frequencies in (a), and the resulting range of predicted cavity shifts in (b) and (c).

with hadronic and weak contributions added, and assuming no electron substructure. Impressive calculations, summarized in [10], give exact C_2, C_4, and C_6, a numerical value and uncertainty for C_8, and a small $a_{\mu\tau}$.

A companion Letter [10] announces a new determination of α, from the measured g and Eq. (6),

$$\alpha^{-1} = 137.035\,999\,710\,(90)\,(33)\,[0.66\ \text{ppb}][0.24\ \text{ppb}],$$
$$= 137.035\,999\,710\,(96)\,[0.70\ \text{ppb}]. \quad (7)$$

The first line gives the experimental uncertainty first and the QED uncertainty second, including an estimated contribution from a yet uncalculated C_{10} [10]. The total 0.70 ppb uncertainty is 10 times smaller than for the next most precise methods [Fig. 1(b)]—determining α from measured mass ratios, optical frequencies, together with either Rb [11] or Cs [12] recoil velocities.

The most stringent test of QED (one of the most demanding comparisons of any calculation and experiment) continues to come from comparing measured and calculated g, the latter using an independently measured α as an input. The new g, compared to Eq. (6) with α(Cs) or α(Rb), gives a difference $|\delta g/2| < 15 \times 10^{-12}$. Details and a discussion are in [10]. The small uncertainties in $g/2$ will allow a 10 times more demanding test if ever the large uncertainties in the independent α values can be reduced. The prototype of modern physics theories is thus tested far more stringently than its inventors ever envisioned [20], with better tests to come.

The same comparison of theory and experiment probes the internal structure of the electron [1,10]—limiting the electron to constituents with a mass $m^* > m/\sqrt{\delta g/2} = 130\ \text{GeV}/c^2$, corresponding to an electron radius $R < 1 \times 10^{-18}$ m. If this test was limited only by our experimental uncertainty in g, then we could set a limit $m^* > 600$ GeV. These high energy limits seem somewhat remarkable for an experiment carried out at 100 mK.

Are experimental improvements possible? A reduction of the 0.76 ppt uncertainty of the measured electron g seems likely, given that this fully-quantum measurement has only recently been realized. Time is needed to study the line shapes and cavity shifts as a function of magnetic field, to improve cooling methods, and to make the magnetic field more stable.

In conclusion, greatly improved measurements of the electron magnetic moment and the fine structure constant, and a sensitive probe for internal electron structure, come from resolving the lowest cyclotron and spin levels of a one-electron quantum cyclotron. A self-excited oscillation of the electron reveals one-quantum transitions. A cylindrical Penning trap cavity narrows resonance lines by inhibiting spontaneous emission. Electromagnetic modes of this understandable cavity geometry, probed with synchronized electrons, shift g in a measurable way that can be corrected. The new $g/2$ differs from a long accepted value by 1.7 standard deviations, and its fractional uncertainty of 7.6×10^{-13} is nearly 6 times smaller. The new α has an uncertainty 10 times smaller than that from any other method to determine the fine structure constant.

Measurement details and a preliminary analysis are in a thesis [21]. S. Peil, D. Enzer, and K. Abdullah contributed to earlier versions of the apparatus, and J. MacArthur gave electronics support. Useful comments came from G. Feldman, D. Hertzog, T. Kinoshita, P. Mohr, L. Roberts, B. Taylor, and R. S. Van Dyck, Jr. The NSF AMO program provided long-term funding.

*Present address: University of Chicago, Chicago, IL 60637, USA.
†Present address: Oak Ridge National Laboratory, Oak Ridge, TN 37831, USA.
‡Electronic address: gabrielse@physics.harvard.edu

[1] S. J. Brodsky and S. D. Drell, Phys. Rev. D **22**, 2236 (1980).
[2] A. Rich and J. C. Wesley, Rev. Mod. Phys. **44**, 250 (1972).
[3] R. S. Van Dyck, Jr., P. B. Schwinberg, and H. G. Dehmelt, *The Electron* (Kluwer, Netherlands, 1991).
[4] R. S. Van Dyck, Jr., P. B. Schwinberg, and H. G. Dehmelt, Phys. Rev. Lett. **59**, 26 (1987).
[5] P. J. Mohr and B. N. Taylor, Rev. Mod. Phys. **72**, 351 (2000); Rev. Mod. Phys. **77**, 1 (2005).
[6] S. Peil and G. Gabrielse, Phys. Rev. Lett. **83**, 1287 (1999).
[7] G. Gabrielse and H. Dehmelt, Phys. Rev. Lett. **55**, 67 (1985).
[8] B. D'Urso, R. Van Handel, B. Odom, D. Hanneke, and G. Gabrielse, Phys. Rev. Lett. **94**, 113002 (2005).
[9] G. Gabrielse and F. C. MacKintosh, Int. J. Mass Spectrom. Ion Processes **57**, 1 (1984).
[10] G. Gabrielse, D. Hanneke, T. Kinoshita, M. Nio, and B. Odom, Phys. Rev. Lett. **97**, 030802 (2006).
[11] P. Cladé, E. de Mirandes, M. Cadoret, S. Guellati-Khélifa, C. Schwob, F. Nez, L. Julien, and F. Biraben, Phys. Rev. Lett. **96**, 033001 (2006).
[12] V. Gerginov, K. Calkins, C. E. Tanner, J. McFerran, S. Diddams, A. Bartels, and L. Hollberg, Phys. Rev. A **73**, 032504 (2006).
[13] G. W. Bennett *et al.*, Phys. Rev. D **73**, 072003 (2006).
[14] L. S. Brown and G. Gabrielse, Phys. Rev. A **25**, 2423 (1982).
[15] L. S. Brown and G. Gabrielse, Rev. Mod. Phys. **58**, 233 (1986).
[16] L. S. Brown, Ann. Phys. (N.Y.) **159**, 62 (1985).
[17] D. G. Boulware, L. S. Brown, and T. Lee, Phys. Rev. D **32**, 729 (1985).
[18] L. S. Brown, G. Gabrielse, K. Helmerson, and J. Tan, Phys. Rev. Lett. **55**, 44 (1985).
[19] J. Tan and G. Gabrielse, Phys. Rev. Lett. **67**, 3090 (1991).
[20] F. Dyson (private communication).
[21] B. Odom, Ph.D. thesis, Harvard University, 2004.